*Standard Article*

# A rate-of-injection model for predicting single and double injection with or without fusion

**Pascal Tetrault**[ID] **and Patrice Seers**

## Abstract

Models used to predict the instantaneous injected fuel mass are of varied interest in automotive applications, including for providing inputs to CFD calculations or for engine control. While multiple injection strategies are now commonly used in diesel engines, the overall approach may be susceptible to injection fusion, which is defined as two successive injections that are partly or totally coupled due to the short time interval between each event. In this work, a new model to predict the instantaneous mass flow rate from a diesel injector is proposed based on the analytical solution of a first-order linear dynamic system exposed to an impulsion. Experiments are also conducted to quantify the main injection characteristics of a solenoid indirect-action injector under different injection pressures, backpressures and injection durations, representing a total of 33 different conditions. From these results, a model is proposed and validated against experimental data using a single injection strategy. Then, the model is enhanced to predict split injection with and without injection fusion. Successful comparisons are realized between the model and the experiment. The model is then used to successfully simulate a piezoelectric injector experiencing different levels of fusion available in the literature so as to illustrate the universality of the proposed approach.

## Introduction

The injection strategy, and more specifically, the instantaneous fuel mass flow rate and the total mass injected, are among the most important parameters in research pertaining to engine performance and emission. To extract these values, the literature presents various approaches that differ in complexity. The most complex among these involve three-dimensional computational fluid dynamics, and are used by the likes of Chouak et al.,[1] who modeled needle displacement using CFD. The 1D model, based on detailed information on the injector geometry and components, represents another approach, where the dynamic response and interaction of the phenomena taking place within the injector are considered using dedicated software[2,3] or by solving a set of Equations.[4,5] Simpler approaches emphasize the end results based on proper equations and correlations. In the latter category, the goal is generally to obtain the rate of injection (ROI), which becomes a useful input to a fuel spray CFD model or to thermodynamic engine performance prediction models. Moreover, depending on its complexity, an instantaneous mass flow rate model could be integrated into the electronic control unit of the engine to predict injected fuel mass as part of the control strategy. In some formulations, the model uses the common rail fuel pressure as an input or can be adapted to model direct gasoline injection with little modifications, as in the model proposed by Payri et al.[6] As the main purpose of this work is to propose a new 0D model of the ROI capable of predicting split injection, recent works pertaining to predictive ROI models are presented in what follows.

Mechanical Engineering Department, École de technologie supérieure, Montreal, QC, Canada

**Corresponding author:**
Pascal Tétrault, Mechanical Engineering Department, École de technologie supérieure, 1100 rue Notre Dame Ouest, Montreal, QC H3C1K3, Canada.
Email: pascal.tetrault.1@ens.etsmtl.ca

A 1D numerical model that considers the solenoid winding of the solenoid as well as the different fuel passages and chambers within the injector was proposed by Ferrari et al.[7] The model has been used to study rate-shaping injection strategies and their effect on the injected mass. Kim et al.[2] also used a similar model to study the effect of fuel viscosity and density under low temperature condition on the rate of injection. They reported that increases in fuel viscosity delayed the start of injection and resulted in lower ROI and injection durations. A similar approach was used to isolate the impact of biodiesel properties on the ROI of a multiple injection strategy, demonstrating that increasing the bulk modulus may decrease the mass injected of the post injection.[3]

Perini et al.[8] proposed an ROI model based on an iterative solution procedure to obtain a specific total injected mass. Armed with minimal knowledge of the injector configuration, the model generates the necessary input to feed a fuel spray CFD calculation. They divided the injection process into four phases: (1) needle transient lift, (2) full needle lift with hydraulic transient flow and (3) full needle lift with near steady-state flow and maximum fuel flow velocity. Finally, there was (4) the needle closing phase. Each phase had its own velocity equation and the model was validated against experimental results for single injections of different durations and different injection pressures while double injection strategies having long time intervals between injection (DT) were also successfully modeled.

Another approach to modeling ROI is presented in Payri et al.[6] to estimate the injected fuel mass of single and multiple injection strategies using rail pressure signals. The purpose of the model is to carry out a real-time estimation of the total fuel injected during engine testing. The model is based on the segmentation of the shapes of the main and pilot injection profiles into a simpler form in a bid to find representative mathematical expressions. For example, second-order Bezier functions are used to curve the corner of the trapezoid representing the main injection event. Overall, the model is able to predict within 8% the total mass injected for a pilot injection strategy, illustrating the ability of this approach to represent the ROI.

Soriano et al.[9] pursued a similar approach by assimilating the ROI profile into a triangle. Their approach consists in determining the ROI using a similar slope with a positive value on the ascent side of the ROI and a negative value on the descent side. Moreover, the slope is a function of the difference between the injection pressure ($P_{inj}$) and the backpressure ($P_{back}$). Double injection was modeled with enough DT allowing separation between each injection and thus preventing injection fusion.

Because multiple injection strategies are often used in diesel engines, it may therefore be possible to have partial or total merging between two successive injections in some of the approaches. This is because the time interval between the electrical command of the two distinct injection events is too short and is responsible for hydraulic instability, and thus leads to excessive fuel mass being injected.[10] Injection fusion may also result from changes in the injector's behavior over its lifespan. In this context, for example, Payri et al.[11] conducted an experimental study on the aging process of an injector using multiple injection strategies. They observed that the ROI was lower and the injection duration longer after aging, resulting in an altered injected mass that could lead to injection fusion over short dwell times. Complex injector modeling efforts have shown that there is a time interval limit between injections that leads to fusion, which depends on the first injection needle closure delay and the needle opening delay of the next injection.[10] During engine injection calibration, injection fusion strategies can be used to offer flexibility in the rate of injection implementation.[12] In the presence of fusion, an injection strategy can be beneficial for the soot-NOx tradeoff at medium engine speeds and loads[12] or for $NO_x$-brake-specific fuel consumption (BSFC) tradeoffs.[13] Recent experiments by d'Ambrosio et al. with a diesel engine have shown that at medium loads, a very short DT decreases combustion noise and offers lower BSFC than other advanced injection strategies, such as boot injection.[14]

Considering the importance of pollutant emission and that fusion injection may be beneficial to diesel engine fuel consumption, the objective of this work is to propose a simple model that allows predicting the ROI for single and double injection with and without the presence of fusion. Proposing a simple ROI model is of interest because it can be easily implemented to predict CFD calculation inputs[8,15] or to predict, at the ECU, the injected fuel mass using the injection pressure.[16]

The paper first presents the experimental setup and injection conditions. Then, experimental results are analyzed, followed by the model description. A comparison between the model and experimental results is presented, and then a comparison between the model and experimental data available in the literature is made to illustrate the versatility of the proposed model. Finally, the main findings are highlighted.

## Experimental setup

An in-house Bosch tube method apparatus was used to characterize the instantaneous mass flow rate of the injector, similar to Kim et al.[2] The method involves injecting fuel at one end of a long tube filled with pressurized fuel. The theoretical foundation of this method is based on the conservation of mass and momentum across a pressure wave of amplitude $dP$ that allows linking the pressure to the injected mass flow rate as per equation (1). The equation was fully derived originally by Bosch[17] while Ferrari and Zhang[18] and the Appendix A, herein, present the main steps leading to the equation. In equation (1), $a$ is the speed of sound in the fuel and S is the tube inner surface area. Because

the derived equation is valid for a single wave, the experimental time frame is limited by the measuring tube length to prevent wave superposition (8 ms on the apparatus used herein).

$$\dot{m}(t) = \frac{S}{a}P(t) \tag{1}$$

Near the injector location, a piezoresistive pressure sensor (Kistler 6061) and a charge amplifier (Kistler 5010a) record the pressure wave appearance due to the injection. At the other tube extremity, a valve allows controlling the reflected pressure wave intensity that will be detected by the amplified pressure sensor. The temperature and static pressure of the diesel fuel are also measured. The instantaneous injection mass flow rate can be calculated if the tube area and the speed of sound of the fuel are known. The latter is extracted from the time interval between the emitted and the reflected pressure wave detected by the pressure sensor and the tube length.

The experiments were conducted using a common rail injection system with a solenoid indirect action Delphi injector. The injector possesses 5–140 μm diameter orifices, and can be operated with a maximum injection pressure of 160 MPa. The common rail was fed with pressurized diesel fuel using an air driven liquid pump (Haskel DSHF-300), while the fuel pressure and temperature were measured using a piezoresistive high-pressure sensor (Kistler 4067) located in the injector feeding pipe. The injector command was generated using an injector module (NI-9751) connected to a CompactRio chassis (CRIO-9074). The chassis also includes a 16-bit acquisition card (NI-9222) that enabled acquiring the signals of the different sensors at a 250 kHz sample rate.

Data post-treatment was performed using Matlab, in which the inherent noise of this experimental approach[19] is filtered. The filtering of the raw pressure signal is followed by a second means-centered window filter over five values. Other approaches have been tested, including using a Butterworth second-order filter, but they offer no marked difference in terms of the injected fuel mass, while being computationally expensive. Overall, the method used herein is similar to that of Bowers and Foster,[20] who used a means-centered window filter using nine values. An uncertainty analysis of the instantaneous mass flow rate was conducted on the experimental setup following the methodology presented in ISO[21], Abernethy et al.,[22] and Le[23] This statistical method is applied to equation (1) and is based on the cumulative impact of the instrument chain reported uncertainties. An uncertainty equal to 2.8% was found for an instantaneous mass flow rate of 12 g/s when considering a 95% confidence interval. The time average of the shot-to-shot standard deviation is within 2% of the steady state mass flow rate, and its instantaneous value is maximum at the start of the second injection.

**Table 1.** Experimental conditions.

| | |
|---|---|
| Injection pressure | 600–1600 bar |
| Back pressure | 1–30 bar |
| Fuel temperature | 303 K |
| Single injection | 0.2–2 ms |
| Double split injection | 0.2–0.500 ms |

Different injection pressures and backpressures were used in combination with single short- and long duration injections, as well as split double injection strategies, characterized by two equal energization time (ET) injections. Both the injection duration and the pressures involved during the experiments are presented in Table 1. Overall, 33 experimental conditions were explored and were repeated 10 times, and the average values are presented in the table.

## Results

### Experimental results

To facilitate the analysis of the results, an adimensional time ($t^*$) is defined by equation (2) and considers the injector opening delay (*IOD*) allowing to set the hydraulic time of the injection process to zero irrespective of the injection conditions. This adimensionalization facilitates the model definition in the next section and has the advantage of displaying changes in the initial instantaneous mass flow rate associated with each measurement.

$$t^* = \frac{t - IOD}{IOD} \tag{2}$$

### Single injection

*Effect of injection pressure.* Figure 1 presents the effect of $P_{inj}$ on the discharge coefficient ($C_d$) of the injector, for different injector energizing times (ET1) of single injections. It is observed that $C_d$ is similar to the value reported by Arcoumanis et al.[24] and shows that the injection pressure does not significantly impact $C_d$ during a transient mass flow rate increase. Moreover, the opening (not shown) and closing delays are of the same order of magnitude as the ones reported by Catania et al.[10] However, the use of equation (2) for the adimensional time leads to the effective injection duration to increase as the $P_{inj}$ increases while the injector opening and closing delays decrease and increase, respectively. This observation is in concordance with the modeling results of Ferrari et al.[12] Moreover, the experimental results show that the injector closing delay increases as the injection duration increases – until a long injection duration (above 2 ms) is reached. This behavior is linked to the fact that when the injection duration is long enough for the needle lift to reach its maximum value, the closing delay has reached its final
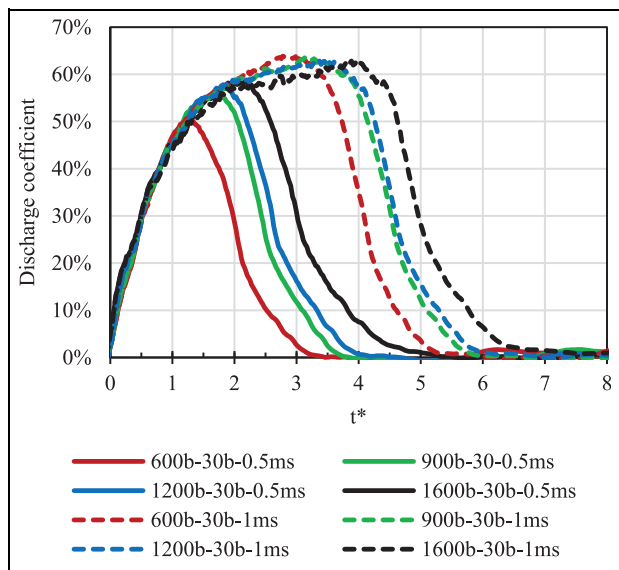
**Figure 1.** Experimental discharge coefficients of single injection for different $P_{inj}$ and ET1 and a $P_{back}$ of 30 bar as a function of adimensional time. Legend for each experimental condition is $P_{inj}$–$P_{back}$-ET1.
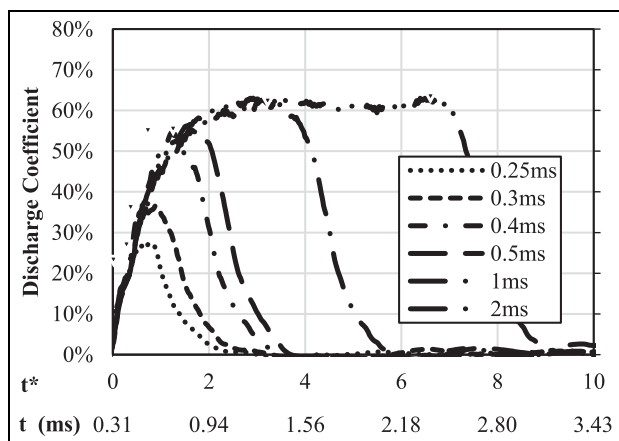


**Figure 2.** Discharge coefficients of single injections for different ET1. Test conditions: $P_{inj}$ of 900 bar and $P_{back}$ of 15 bar.

value.[12] Finally, the experimental results indicate that $P_{inj}$ hardly impacts the $C_d$ modulus during injector closing using the same adimensional time scale $t^*$, at least for $P_{inj}$ covered herein (figure not shown, for brevity). This is in concordance with the findings of Kastengren et al.,[25] who stated that the needle speed is slightly dependent on $P_{inj}$ during closing.

*Effect of injection duration.* Figure 2 presents $C_d$ of different ET, with the small triangle identifying the start of the flow rate reduction phase, which approximately corresponds to the junction point between the experimental curves and the end of the electrical injection command. It is observed that for ET shorter than 1 ms, the steady-state regime is not attained and that the
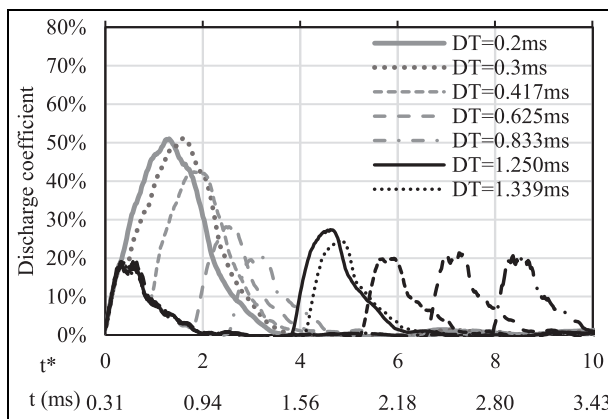


**Figure 3.** Discharge coefficients of double split injection (ET of 0.2 ms) for different DT. Test conditions: $P_{inj}$ of 900 bar and $P_{back}$ of 30 bar.

injection process is achieved under transient needle displacements. Figure 2 also illustrates that the initial increase of $C_d$ with time is independent of the ET duration as all curves are superimposed.

### Double injection

We now look into double injection in a bid to characterize the impact of the time interval between the beginning of two successive injections (DT), which is defined that way to be consistent with the model to be presented in a later section. Figure 3 presents the experimental results obtained with a split injection of 0.2 ms, with DT varying from 0.2 to 2.5 ms. Contrary to Ferrari and Mittica,[12] who defined a fusion of injection when there is an interaction between two successive injections, three coupling modes are defined herein, which will be helpful in the definition of the model in the next section. The first mode represents a fusion between two successive injections, as can be observed for DT shorter than 0.3 ms. The fusion means that both ETs generate a $C_d$ profile having a single maximum value, similarly to the case with a DT of 0.2 ms. The second coupling mode is a partial fusion, and is defined by a $C_d$ having two maximums without a zero-mass flow rate between them, such that the end of the first injection cannot be distinguished from the beginning of the second injection, as in the case of a DT of 0.417 ms in Figure 3. Finally, a third mode is identified in Figure 3, and is defined for cases where $C_d$ returns to zero between both injections, but for which the second injection reaches a higher $C_d$ than the first, such as in the case of DTs of 1.25 and 1.339 ms. Tests were also performed with a split injection having an ET of 0.5 ms, as illustrated in Figure 4. It can be seen that the first two fusion modes identified above are observable and that a DT of 1.339 ms is necessary to differentiate between the presence and the absence of fusion. Moreover, due to the longer duration of each injection, the $C_d$, in the presence of fusion (see DT of 0.625 ms), reaches the nominal value associated with a single long injection duration.
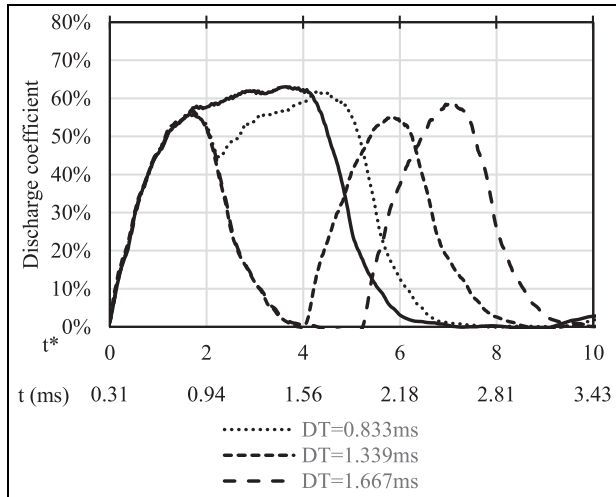
**Figure 4.** Discharge coefficients of double split injections (ET of 0.5 ms) for different DT. Test conditions: $P_{inj}$ of 900 bar and $P_{back}$ of 30 bar.
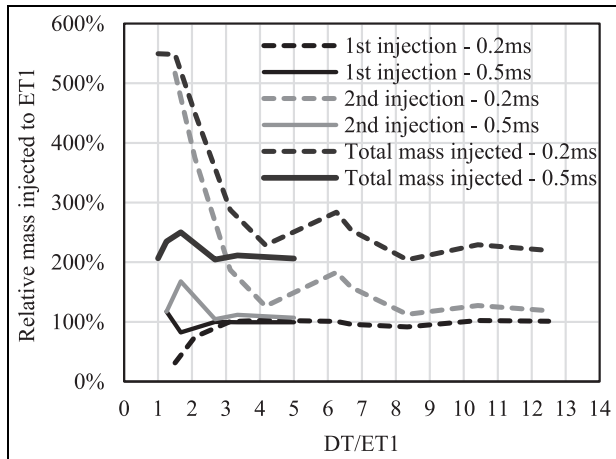


**Figure 5.** Relative total mass injected for double split injection with respect to a single injection having the same ET. Test conditions: $P_{inj}$ of 900 bar and $P_{back}$ of 30 bar.



**Figure 6.** Influence of DT/ET1 on the injector opening delay of the second injection.

To illustrate the impact of the fusion, the relative injected mass is calculated as the ratio of the mass injected during the split injection to the one from a single injection. Hence, a split injection comprised of two 0.2 ms injections should have a relative mass of 200% of a single injection of 0.2 ms in the absence of fusion or interaction between both injections. Results are presented in Figure 5 as a function of DT/ET1. First, it is observed that the shortest injection (0.2 ms) studied herein is much more sensitive with respect to the relative injected mass since the needle's transient displacement plays a major role during the injection process as the nominal mass flow rate is not reached, contrary to a split injection, which consists of two successive 0.5 ms injections. Second, the first injection is statistically equivalent to a single injection of the same duration if DT/ET1 is equal to or > 2 due to the difficulty of
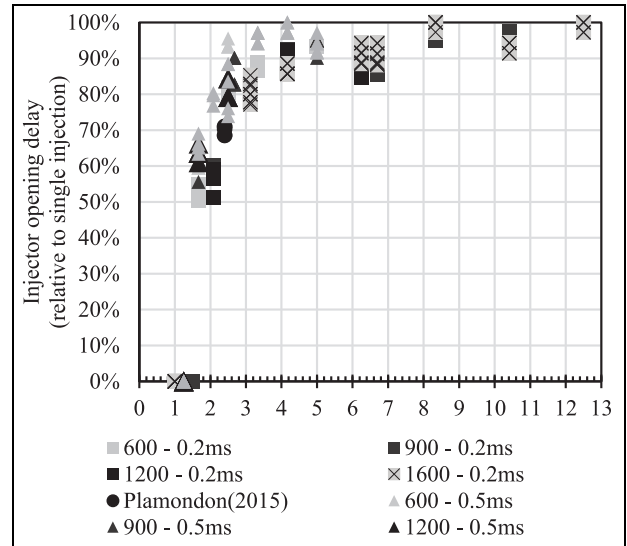
determining the injected mass associated with the first and second injections under DT/ET1 < 2. Third, the fusion between injections is maximum at around a DT/ET1 of 1.5 and can generate an increased relative mass of more than five times the equivalent of a single injection. An increase in injected mass has also been reported experimentally by Ferrari and Mittica[12] and Herfatmanesh.[26]

From the experimental results, it can be seen that the injector opening delay of the second injection is highly sensitive for DT/ET1 < 2, which is obtained in cases where a partial or complete fusion of both injections has been observed. For DT/ET1 > 4, it can be considered that the opening delay is equivalent to the delay associated with a single injection. The shorter opening delay observed in Figure 6 at a DT/ET1 of 6.25 corresponds to the third coupling mode (higher $C_d$ of second injection even if the injector closes between both injections) observed in Figure 3. Finally, the closing delay of the second injection is reported for the split injection tested in Figure 7 and shows a dependence on DT/ET1, the injection duration (ET2) and $P_{inj}$, contrary to a single injection, for which the closing delay is only a function of $P_{inj}$ and ET. Thus, due to its greater sensitivity to both parameters, the closing delay shows more variations for DT/ET1 below 3, while it tends to the value of a single injection at higher DT/ET1, with the exception of when DT/ET1 is equal to 6.25 and 6.75, in which case the closing delay increases (Figure 7). Figure 6 already showed a decrease of the opening delay. This behavior explains the increase of total mass injected in Figure 5 and where it is observed an extreme case (split injection with ET1 = ET2 = 0.2 ms) of a relative mass of 550% with respect to a single injection which is also equivalent to 2.5 times the expected mass of a split injection in the absence of fusion.
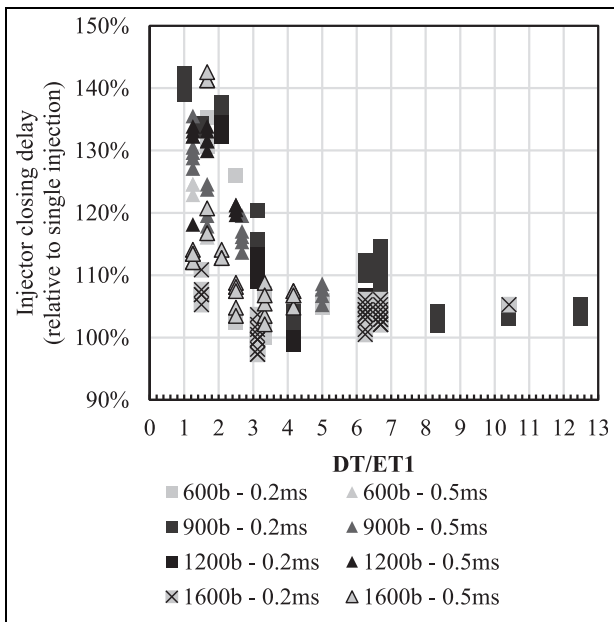
**Figure 7.** Influence of DT/ET1 on the injector closing delay of the second injection.

## Empirical model

Based on the above experimental observation, an empirical model is proposed, and is based on the analytical solution of the response of a first-order linear dynamic system to an impulsion.[27] Thus, the model uses an exponential function to predict the experimental discharge coefficient $\left( C_d = \frac{\dot{m}_f}{A_{nozzle}\sqrt{2\rho_f \Delta P}} \right)$ associated with a phase identified in the experimental results of the injection process. Each phase of this process is illustrated in Figure 8, which also presents the electrical command associated with each injection, the temporal parameters of the model as well as the definition of DT. The first phase is the injector opening delay (IOD), which characterizes the time between the beginning of the electrical command and the appearance of fuel injection. In phase 2, we have the increasing mass flow rate, which lasts until after the end of the electrical injection command, as identified in the experimental results. This second phase also considers the steady-state mass flow rate for long injection durations. Finally, the third phase is the injector closing delay (ICD) phase, and is associated with a decreasing mass flow rate until the effective end of injection. The latter is defined as the time when a threshold of 0.1% of the nominal mass flow rate is reached. The second injection is represented by the fourth and fifth phases in Figure 8 and is thus defined similarly to the first injection.

The proposed empirical equations are developed using the experimental results of single injections (see Table 1 for experimental conditions) to statistically calibrate the ramp-up period. Following the opening delay, the second phase is represented by equation (3) and ensures a constant mass flow rate increase as a function of adimensional time ($t^*$) until the steady-state value ($C_{d\_SS}$) is reached. The injector opening delay is represented by an offset of the injector response to an electrical command through the variable $t_{iod}$ whose coefficients have to be calibrated experimentally to the studied injector. Experimentally, $t_{iod}$ (in seconds) is a weak function of the injection pressure (in Pa), as expressed by equation (4) with $t_{iodmax} = 0.0004$ and $E = 6 \times 10^{-13}$ for the studied injector. Herein, $t_{iodmax}$ is obtained at an injection pressure of 600 bar. In
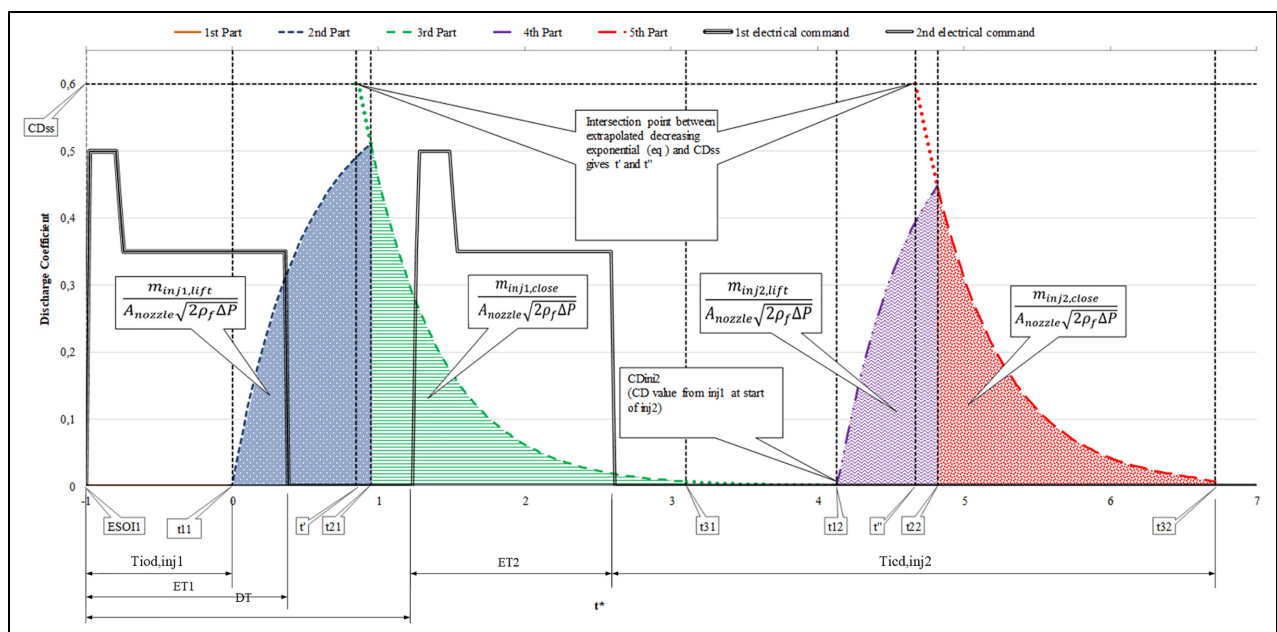


**Figure 8.** Piece-wise model graphical nomenclature of the mass flow rate/discharge coefficient $\left( C_d = \frac{\dot{m}_f}{A_{nozzle}\sqrt{2\rho_f \Delta P}} \right)$ and injector's electrical commands as a function of adimensional time (t*) (Dimensions not to scale).

equation (3), $\tau_{lift}$ is the time constant of the injector to reach a steady-state mass flow rate and will be defined shortly. $C_{d\_ini}$ is the initial discharge coefficient, which is equal to zero for a single injection and the first injection of a double injection strategy, while for the second injection, its value is a function of the degree of fusion between both injections. Injections are defined as fully fused if $t_{12} \leqslant t_{21}$ (see Figure 8). In such a case, the lifting phase of injection 1 is prolonged to $t_{22}$, skipping the third and fourth phases in Figure 8.

General form $\left( C_{D_{lift}}(t) = C_{D.SS} + (C_{D.ini} - C_{D.SS})e^{-\left(\frac{t - t_{iod}}{\tau_{lift}}\right)} \right)$

Injection 1

If $t_{12} > t_{21}$    $C_{D,inj1,lift}(t) = C_{D_{lift}}(t)$
      with $C_{D.ini} = 0$, $t_{iod} = 0$ and for $0 \leqslant t \leqslant t_{21}$

If $t_{12} \leqslant t_{21}$    $C_{D,inj1,lift}(t) = C_{D_{lift}}(t)$
      with $C_{D.ini} = 0$, $t_{iod} = 0$ and for $0 \leqslant t \leqslant t_{22}$

Injection 2

If $t_{12} > t_{21}$    $C_{D,inj2,lift}(t) = C_{D_{lift}}(t)$
      with $C_{D.ini} = C_{Dini,2}$, $t_{iod} = t_{12}$ and for $t_{12} \leqslant t \leqslant t_{22}$

If $t_{12} \leqslant t_{21}$    $C_{D,inj2,lift}(t) = 0$

$$(3)$$

$$t_{iod} = t_{iodmax} - E \cdot P_{inj} \tag{4}$$

Using the same approach, the discharge coefficient for the last phase of the injection process is based on the single injection after the end of the electrical command. A decreasing exponential function is used as expressed by equation (5), where $T$ ensures a continuity of $C_d$ at the peak mass flow rate. The values of $T$ for the first and second injection are specified with equation (5). From the experimental results, $\tau_{close}$ represents the time constant for the needle to return to its closing position from the start of the flow rate reduction phase, as identified in Figure 2, for example.

General form    $C_{D_{close}}(t) = C_{D\_SS}e^{-\left(\frac{t - T}{\tau_{close}}\right)}$

For injection 1

If $t_{12} > t_{21}$    $C_{D,inj1,close}(t) = C_{D_{close}}(t)$
          with $T = t'$ and for $t_{21} \leqslant t \leqslant \min(t31, t12)$

If $t_{12} \leqslant t_{21}$    $C_{D,inj1,close}(t) = 0$

For injection 2    $C_{D,inj2,close}(t) = C_{D_{close}}(t)$
          with $T = t''$ and for $t_{22} \leqslant t \leqslant t_{32}$

$$(5)$$

In equations (3) and (5), two characteristic times for the opening delay ($\tau_{lift}$) and the closing delay ($\tau_{close}$) of the injector are required, and both are a function of the IOD and ICD, respectively. ICD has been observed experimentally to be a function of ET and $P_{inj}$. Moreover, it has been observed experimentally (see Figure 7) that ICD is constant once ET is above 1 ms. This particular effect is taken into account by a sigmoid as presented by equation (6), for which a 95% coefficient of correlation
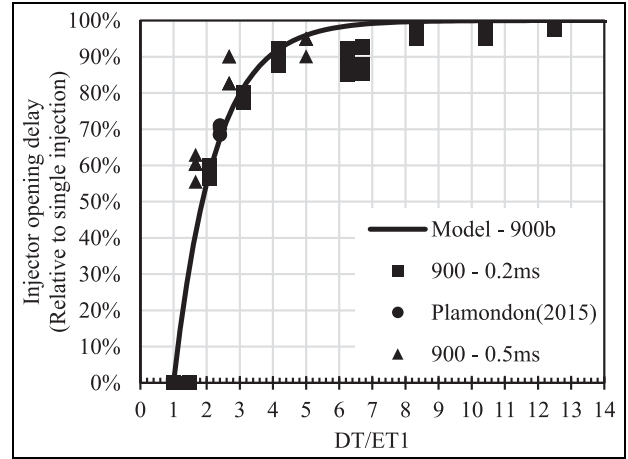


**Figure 9.** Injector opening delay of the second injection in the presence of coupling (fusion) with the first injection. Experimental results (symbols) and equation (6) (line).

is obtained with the experimental results (data not shown, for brevity) of single injections when the empirical coefficients A = 0.0011, B = 4990, C = $7.5 \times 10^{-9}$, and D = 1.28 are used.

$$t_{icd}\left(P_{inj}, ET\right) = \frac{A}{1 + e^{\left(-B \cdot ET - C \cdot P_{inj} + D\right)}} \tag{6}$$

In the absence of fusion, IOD is constant and equal to $t_{iod}$ of a single injection given by equation (4). For double injection strategy cases, it has been observed experimentally that the injector opening delay of the second injection varies depending on the presence or absence of fusion between injections. Moreover, the analysis of experimental results has shown that DT/ET1 can be used to predict the presence of fusion between injections. Hence, IOD is calculated with equation (7) and allows representing the absence or presence of fusion. In the latter case, the term $\left(\frac{ET1}{ET2}\right)^k$ allows to account for the fusion behavior by adjusting the value $k$ to the injector dynamic. In equation (6), it is assumed that a double injection having a DT/ET1 equal to 1 has the same behavior as a single injection having an energization time equal to the sum of both injection energization times (ET1 and ET2), and hence, an absence of delay between injections. On the other hand, a strategy with a DT/ET1 that tends to infinity will show the behavior of two distinctive single injections. This behavior is illustrated in Figure 9, which shows a satisfactory agreement.

$$t_{iod,fusion} = \left[1 - e^{\left(0,8\left(\frac{ET1}{ET2}\right)^k \left(1 - \frac{DT}{ET1}\right)\right)}\right] t_{iod} \text{ with } k = 1$$

$$(7)$$

The characteristic times for the needle opening ($\tau_{lift}$) and closing ($\tau_{close}$) are defined based on experimental results, where a proportionality is observed between these variables and IOD. Moreover, the experimental results show that the slope of $C_d$ during injector

opening and closing is not sensitive to ET. Finally, it is observed, experimentally herein, that $\tau_{lift}$ and $\tau_{close}$ are nearly identical and that the same behavior can be observed with the results from Ferrari and Zhang[7] who used a different injector technology. They are, thus, defined as equal, as per equation (8), and will be referred to as $\tau$ hereafter, such as in equation (10). This simplification allows an analytical solution for the peak $C_d$ occurrence time of both injections but is not mandatory if a numerical approach is used to solve equation (10).

$$\tau = \tau_{lift} = \tau_{close} = 0.5\,IOD \qquad (8)$$

Finally, the coupling effect on the closing process between the first and second injections is represented by equation (9), where it can be seen that ICD during fusion is a function of ET1, ET2, and DT. In equation (9), the term $\left(\frac{ET1}{ET2}\right)^k$ allows to account for the fusion behavior by adjusting the value $k$ to the injector dynamic. A value of k equals to 1 is used and shows a good agreement with the experimental results herein as well as with the data of Ferrari and Zhang[7] that are presented in a later section. With equation (9), a DT/ET1 of unity will result in a single injection having a duration representing the sum of both injections. Equations (4), (6), (7), and (9) are an empirical simplification of the injector's dynamic response and need experimental data to calibrate and obtain an accurate prediction.

$$t_{icd,fusion} =$$
$$\left[\left(\frac{t_{icd}(ET1 + ET2, P_{inj})}{t_{icd,fusion}(ET2, P_{inj})} - 1\right)e^{\left(\frac{1}{2}\left(\frac{ET1}{ET2}\right)^k\left(1-\frac{DT}{ET1}\right)\right)} + 1\right]t_{icd}$$
with $k = 1$ and $t_{icd}$ from equation 6

$$(9)$$

The above equations (2–9) can be used by themselves to obtain $C_d(t)$ numerically. They can also be integrated analytically over time to enable predicting the total mass injected as per equation (10), which is the sum of the mass injected during each injection phase. This integration necessitates the calculation of a few time constants that are also presented below. These time constants are linked to the temporal position of each phase, such as the opening delay, the transient needle lift, the steady-state flow (if reached) and the transient needle closure. A graphical representation of the geometric significance of the time constants of equation (10) is shown in Figure 8 where the time is adimensionalized using equation (2). Figure 8 also extrapolates the third and fifth phases (decreasing phase) to the steady state discharge coefficient to illustrate the geometrical definition of times constants $t'$ and $t''$ in equation (10).

$$m_f = m_{inj1,lift} + m_{inj1,close} + m_{inj2,lift} + m_{inj2,close}$$

$$m_f = A_{nozzle}\sqrt{2\rho_f\Delta P}\left(\int_{t11}^{t21} C_{D,inj1,lift}(t)\,dt\right.$$
$$+ \int_{t21}^{\min(t31,t12)} C_{D,inj1,close}(t)dt + \int_{t12}^{t22} C_{D,inj2,lift}(t)dt$$
$$\left.+ \int_{t22}^{t32} C_{D,inj1,close}(t)dt\right) \qquad (10)$$

The total mass injected in equation (10) is thus the sum of the fuel of each phase identified in Figure 8. equations (11) and (12), allow calculating the mass injected during the needle lift and closing phases, respectively, of the first injection, while equations (13) and (14) permit the same calculations for the second injection.

If $t_{12} > t_{21}$ $\quad m_{inj1,lift} = A_{nozzle}\sqrt{2\rho_f\Delta P}$
$$\left(C_{Dss}(t_{21} - t_{11}) + \tau C_{Dss}\left(e^{-\left(\frac{t_{21}-t_{11}}{\tau}\right)} - 1\right)\right)$$

If $t_{12} < -t_{21}$ $\quad m_{inj1,lift} = A_{nozzle}\sqrt{2\rho_f\Delta P}$
$$\left(C_{Dss}(t_{22} - t_{11}) + \tau C_{Dss}\left(e^{-\left(\frac{t_{22}-t_{11}}{\tau}\right)} - 1\right)\right)$$

$$(11)$$

If $t_{12} > t_{21}$ $\quad m_{inj1,close} = A_{nozzle}\sqrt{2\rho_f\Delta P}$
$$\left(-\tau C_{Dss}\left(e^{-\left(\frac{\min(t31,t12)-t'}{\tau}\right)} - e^{-\left(\frac{t_{21}-t'}{\tau}\right)}\right)\right)$$

If $t_{12} < -t_{21}$ $\quad m_{inj1,close} = 0$

$$(12)$$

If $t_{12} > t_{21}$ $\quad m_{inj2,lift} = A_{nozzle}\sqrt{2\rho_f\Delta P}$
$$\left(C_{Dss}(t_{22} - t_{12}) - \tau(C_{Dini2} - C_{Dss})\left(e^{-\left(\frac{t_{22}-t_{12}}{\tau}\right)} - 1\right)\right)$$

If $t_{12} < -t_{21}$ $\quad m_{inj2,lift} = 0$

$$(13)$$

$$m_{inj2,close} =$$
$$A_{nozzle}\sqrt{2\rho_f\Delta P}\left(-\tau C_{Dss}\left(e^{-\left(\frac{t_{32}-t''}{\tau}\right)} - e^{-\left(\frac{t_{22}-t''}{\tau}\right)}\right)\right)$$

$$(14)$$

The different time constants associated to the first injection are computed as follows using parameters that have been defined previously.

$$t_{11} = t_{iodmax} - (E \cdot P_{inj}) \qquad (15)$$

$$t_{31} = ET1 + \frac{A}{1 + \exp(-B \cdot ET - C \cdot P_{inj} + D))} \qquad (16)$$

$$t' = \tau\ln(0,001) + t_{31} \qquad (17)$$

$$t_{21} = \tau\ln\left(e^{\frac{t'}{\tau}} - 1\right) \qquad (18)$$

The initial discharge coefficient of the second hydraulic injection ($C_{Dini,2}$) is based on the steady-state value of $C_D$ as given by equation (19).
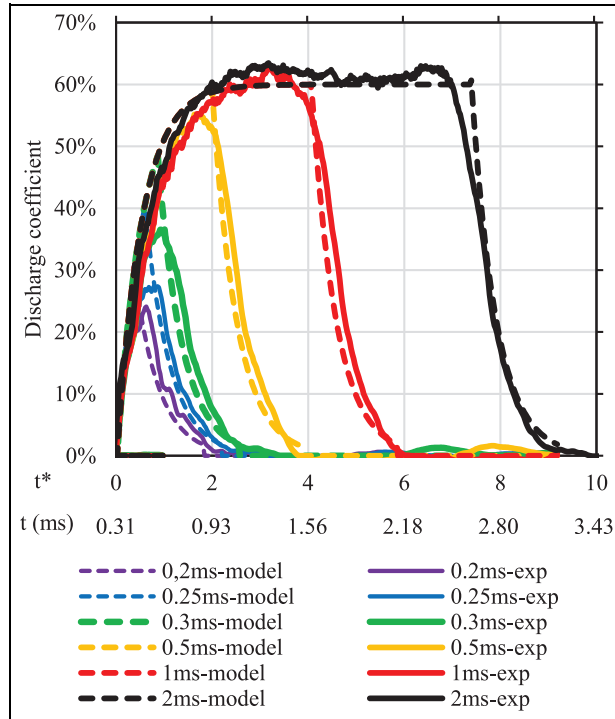
**Figure 10.** Comparison of single injections between experimental results and the proposed model for different ETs. Test conditions: $P_{\text{inj}}$ of 900 bar and $P_{\text{back}}$ of 15 bar.

$$C_{Dini,2} = C_{Dss}\, e^{-\left(\frac{t_{12}-t'}{\tau}\right)} \tag{19}$$

The, the time constants linked to the second injection can be found using equations (20)–(24).

$$t_{12} = DT + \left[t_{iodmax} - \left(E \cdot P_{inj}\right)\right] \cdot$$
$$\left[1 - \exp\left(\frac{1}{1.25}\left(\frac{ET1}{ET2}\right)^{k}\left(1 - \frac{DT}{ET1}\right)\right)\right] \tag{20}$$

$$t_{22} = \tau \ln\left(e^{\frac{t''}{\tau}} - \left(\frac{C_{Dini,2}}{C_{Dss}} - 1\right)e^{\frac{t_{12}}{\tau}}\right) \tag{21}$$

$$t_{32} = DT + ET2 + \left[\frac{A}{1 + \exp\left(-B*ET - C*P_{inj} + D\right)}\right] \cdot$$
$$\left[\left(\frac{ICD(ET1 + ET2)}{ICD(ET2)} - 1\right)\cdot\exp\left(\frac{1}{2}\left(\frac{ET1}{ET2}\right)^{k}\cdot\left(1 - \frac{DT}{ET1}\right)\right) + 1\right] \tag{22}$$

$$t'' = \tau \ln(0,001) + t_{32} \tag{23}$$

Finally, $t'$ and $t''$ given by equations (17) and (23), respectively, are the time constants associated with the moment when $C_d$ is equal to 0.1% of the closing delay.

## Comparison model and experimental results

The above model was programmed in Matlab and its results are first compared to the experimental results obtained herein. Figure 10 presents a comparison between the experimental results and the model for different single injections using a $P_{\text{inj}}$ of 900 bar. These
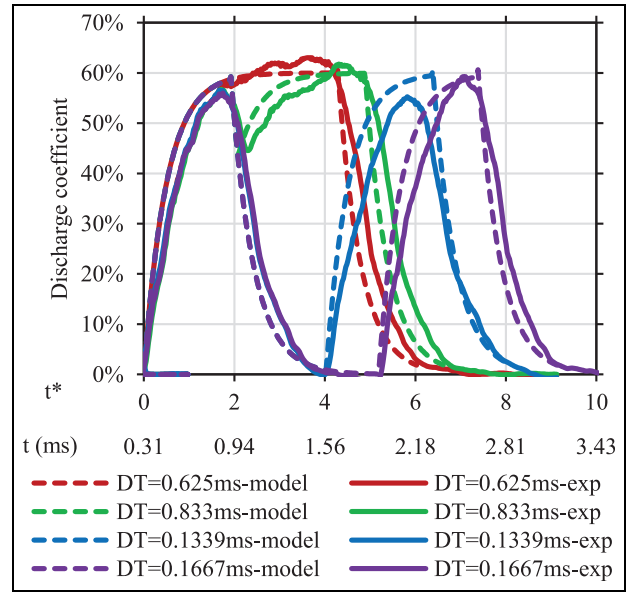


**Figure 11.** Comparison of split injections (ET = 0.5) between experimental results and the proposed model for different DTs. Test conditions: $P_{\text{inj}}$ 900 bar and $P_{\text{back}}$ of 15 bar.
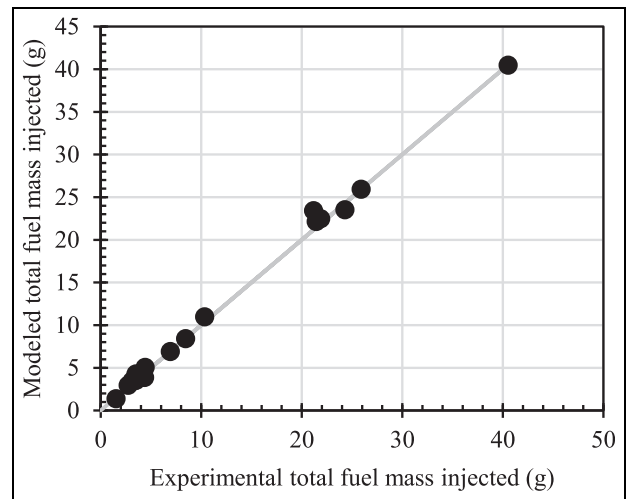


**Figure 12.** Total mass injected of single or double injection: prediction versus experiment results.

single injections are used to calibrate all the model constants, and show a good performance by the model. A maximum overprediction of 12% is obtained by the model on the total mass injected for the shortest injection of 0.2 ms. The accuracy reported herein is similar to the one shown by Kim et al.[2] with injection durations of 0.45 ms and 1 ms using a complex modeling approach (commercial software).

The calibrated model is now used to predict different split injections having an ET of 0.5 ms tested herein, and the results are shown in Figure 11 for a $P_{\text{inj}}$ of 900 bar and different DT. The results show the model's ability to predict the presence or absence of fusion between injections, while the maximum overprediction on the total mass injected is 3% for cases with a DT of 0.625 ms. This is comparable to the value reported in
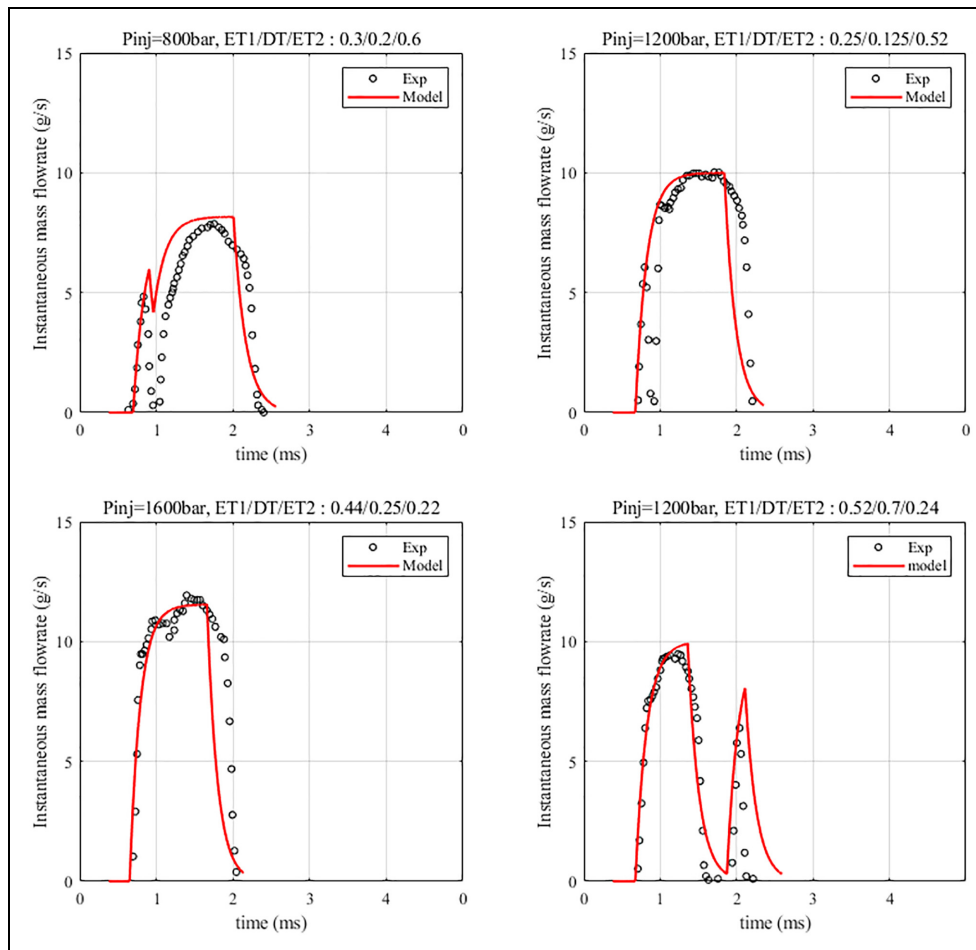
**Figure 13.** Comparison between the proposed model and experimental results of Ferrari and Zhang[7] for different double injection strategies using a piezoelectric diesel injector ($t_{iod,inj1}$ = 0.00036, A = 0.0011, B = 5500, C = 4e-9, D = 1,28 and E = 5,62e-13).

Payri et al.,[6] where a maximum deviation of the total mass injected is lower than 8% for pilot injections. Thus, it can be said that the model allows representing the behavior of the injector for both single and split injection strategies. Moreover, the predicted injected mass shows a good agreement with the experimental results. This can be seen in Figure 12, which compares the predicted total mass injected to the experimental one ($R^2$ = 0.99).

Finally, to show the versatility of the model, two different injection strategies using a piezoelectric injector are now modeled based on experimental results available in the literature. The Pre-Main and Main-Post injection strategies from Ferrari and Zhang[7] using a piezoelectric injector offered enough data to pursue this additional validation of the proposed approach. Their experiments presented mass flow rate measurements using a piezoelectric injector for a fused pilot-main injection and an unfused main-post strategy. While few data were available to determine the different time constants, the proposed model is able to predict the general flow rate behavior, as can be observed in Figure 13 for four (4) different injection strategies. The values of the constants A, B, C, D, and E used in the model are also provided (see figure title) to show the similarity with

the values used above, while it is noted that the injector technology is different. The model shows satisfactory prediction results under the pilot-main injection strategies. However, it overpredicts the injected mass under main-post injection strategies, as illustrated in Figure 13 (bottom-right). This mass overprediction can be attributable to a different fusion behavior under main-post strategies, as reported in Ferrari and Zhang.[7] The proposed model accounts for this behavior by using a $(ET1/ET2)^k$ factor in equations (6), (8), (11), and (15), but additional data would have been necessary to properly calibrate the model. Overall, satisfactory results were obtained, considering the simplicity of the model.

## Conclusion

The paper proposes a new rate-of-injection empirical model based on an analytical solution of a first-order linear dynamic system exposed to an impulsion, and is validated against experimental data. It is thus based on a simple algebraic solution. To support the model validation, experiments have been conducted with simple and split injection strategies over different injection pressures, injection durations, and time intervals between injections. While single injections were

successfully modeled, one of the main features of the model is its ability to predict the double injection mass flow rate even when a fusion of both injections is observed.

The proposed model was developed using an indirect solenoid injector. However, by using data available in the literature, the model shows its universality by allowing to predict the instantaneous mass flow rate of a piezoelectric injector. Finally, the model allows predicting single and double injections with and without fusion.

## Declaration of conflicting interests

## Funding

## ORCID iD

Pascal Tétrault https://orcid.org/0000-0002-5560-6259

## References

1. Chouak M, Mousseau A, Reveillon D, Dufresne L and Seers P. Study of transient effects in the internal flow of a Diesel fuel injector. SAE paper 2015-01-0923, 2015.
2. Kim J, Lee J and Kim K. Numerical study on the effects of fuel viscosity and density on the injection rate performance of a solenoid diesel injector based on AMESim. *Fuel* 2019; 256: 115912.
3. Boudy F and Seers P. Impact of physical properties of biodiesel on the injection process in a common-rail direct injection system. *Energy Convers Manag* 2009; 50: 2905–2912.
4. Chung N, Oh B and Sunwoo M. Modelling and injection rate estimation of common-rail injectors for direct-injection diesel engines. *Proc IMechE, Part D: J Automobile Engineering* 2008; 222: 1089–1101.
5. Plamondon E and Seers P. Development of a simplified dynamic model for a piezoelectric injector using multiple injection strategies with biodiesel/diesel-fuel blends. *Appl Energy* 2014; 131: 411–424.
6. Payri R, Gimeno J, Novella R, et al. On the rate of injection modeling applied to direct injection compression ignition engines. *Int J Engine Res* 2016; 17: 1015–1030.
7. Ferrari A and Zhang T. Influence of the injector setup on digital and continuous injection rate-shaping performance in diesel engine passenger cars. *Energy Convers Manag* 2020; 205: 112259.
8. Perini F, Busch S and Reitz RD. A phenomenological rate of injection model for predicting fuel injection with application to mixture formation in light-duty diesel engines. *Proc IMechE, Part D: J Automobile Engineering* 2020; 234: 1826–1839.
9. Soriano JA, Mata C, Armas O, et al. A zero-dimensional model to simulate injection rate from first generation common rail diesel injectors under thermodynamic diagnosis. *Energy* 2018; 158: 845–858.
10. Catania AE, Ferrari A, Manno M, et al. Experimental investigation of dynamics effects on multiple-injection common rail system performance. *J Eng Gas Turbines Power* 2008; 130: 032806.
11. Payri R, Marti-Aldavari P, Montiel T, et al. Influence of aging of a diesel injector on multiple injection strategies. *Appl Therm Eng* 2020; 181: 115891.
12. Ferrari A and Mittica A. Response of different injector typologies to dwell time variations and a hydraulic analysis of closely-coupled and continuous rate shaping injection schedules. *Appl Energy* 2016; 169: 899–911.
13. d'Ambrosio S and Ferrari A. Exploitation of injection fusion strategies in diesel engines equipped with solenoid injectors. *Int J Engine Res* 2018; 19: 653–667.
14. d'Ambrosio S, Ferrari A, Mancarella A, et al. Effects of rate-shaped and multiple injection strategies on pollutant emissions, combustion noise and fuel consumption in a low compression ratio diesel engine. *Int J Automot Technol* 2020; 21: 197–214.
15. Xu L, Bai X-S, Jia M, et al. Experimental and modeling study of liquid fuel injection and combustion in diesel engines with a common rail injection system. *Appl Energy* 2018; 230: 287–304.
16. Ferrari A and Paolicelli F. An indirect method for the real-time evaluation of the fuel mass injected in small injections in Common Rail diesel engines. *Fuel* 2017; 191: 322–329.
17. Bosch W. The fuel rate indicator: A new measuring instrument for display of the characteristics of individual injection. SAE paper 660749, 1966.
18. Ferrari A and Zhang T. Benchmark between Bosch and Zeuch method–based flowmeters for the measurement of the fuel injection rate. *Int J Engine Res* 2021; 22: 316–327.
19. Manin J, Kastengren A and Payri R. Understanding the acoustic oscillations observed in the injection rate of a common-rail direct injection diesel injector. *J Eng Gas Turbines Power* 2012; 134(12): 122801.
20. Bower GR and Foster DE. *A comparison of the Bosch and Zudch rate of injection meters*. Wisconsin University - Madison Engine Research Center, Wisconsin, USA, 1991.
21. International Organization for Standardization. Measurement of fluid flow: procedures for the evaluation of uncertainties. ISO, 2005.
22. Abernethy RB, Benedict RP and Dowdell RB. ASME measurement uncertainty. *J Fluids Eng* 1985; 107: 161–164.
23. Lee T-W. *Thermal and flow measurements*. CRC Press, FL, USA, 2008.
24. Arcoumanis C, Flora H, Gavaises M, et al. Cavitation in real-size multi-hole diesel injector nozzles. *SAE Technical Paper* 2000-01-1249, 2000.
25. Kastengren A, Powell C, Liu Z, et al. High-speed X-ray imaging of diesel injector needle motion. In: *Proceedings of the ASME 2009 internal combustion engine division spring technical conference. ASME 2009 internal combustion engine division spring technical conference*, Milwaukee, Wisconsin, May 3–6, 2009, pp.247–258. New York: ASME.
26. Herfatmanesh MR, Lu P, Attar MA, et al. Experimental investigation into the effects of two-stage injection on fuel injection quantity, combustion and emissions in a high-speed optical common rail diesel engine. *Fuel* 2013; 109: 137–147.

27. Nise N. *Control systems engineering.* John Wiley & Sons, NJ, USA, 2007.
28. Bosch W. The fuel rate indicator: a new measuring instrument for display of the characteristics of individual injection. *SAE Technical Paper* 660749, 1966.
29. Ferrari A and Zhang T. Benchmark between Bosch and Zeuch method-based flowmeters for the measurement of the fuel injection rate. *Int J Engine Res* 2021; 22(1): 316–327.

# Appendix A

## *Derivation of the theoretical foundation of the Bosch's measuring tube method*

The mathematical foundation of the Bosch's measuring tube method is based on a hydraulic pulse theory of a traveling single pressure wave. The derivation below is from Bosch[28] and Ferrari et al.[29] and is based on a 1D flow within a pipe of constant cross-section, $S$, and a fluid initially at rest. Moreover, it is based on the definition of mass flow rate ($\dot{m} = S \cdot \rho \cdot u$, equation (A1.0)) where $u$ is the velocity at the pressure sensor location.

The derivation considers a moving control volume as illustrated in Figure A1 that follows a pressure wave moving from left to right and traveling at the speed of sound, $a$, such that the flow properties (pressure, velocity, and density) upstream of the wave are thus $P, a, \rho$ while downstream of the wave one found $P + dP, a - du, \rho + d\rho$ as illustrated below. Thus, by applying the mass conservation principle to the control volume:

$$\dot{m}_{in} = \dot{m}_{out} \qquad (A1.1)$$

with

$$\dot{m}_{in} = \rho \, S \, a \qquad (A1.2)$$
$$\dot{m}_{out} = (\rho + d\rho)S(a - du) \qquad (A1.3)$$

Using definitions (A1.2) and (A1.3) are substituted in (A1.1) one obtains (A1.4) where the magnitude of the second-order term ($du \cdot d\rho$) is eliminated.[28]

$$d\rho = \frac{\rho}{a}du \qquad (A1.4)$$

Similarly, the momentum balance across the control volume one obtains equation (A.1.6) where the term $S \cdot dP$ is the external force acting on the control volume responsible for the difference between the inlet and outlet. The general form of the momentum, $\dot{m}u$, is defined as $S\rho U^2$ where $U$ is the velocity as seen from the pressure wave point of view.

$$\dot{m}u_{in} = \dot{m}u_{out} + S \cdot dP \qquad (A1.6)$$

Thus, the momentum quantities are defined per (A1.7) and (A1.8) considering that $U = a$ and $U = a - du$ when entering and exiting, respectively, the control volume.
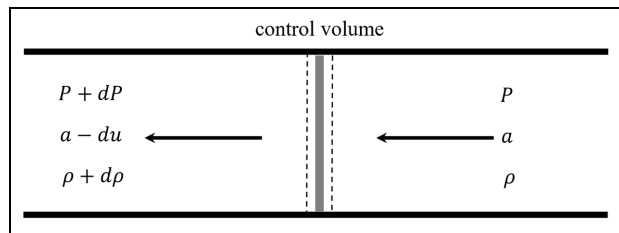
$$\dot{m}u_{in} = \rho S a^2 \qquad (A1.7)$$



**Figure A1.** Pressure wave in a pipe with a moving frame of reference from the wave point of view. From an outside observer, the wave is moving from left to right.

$$\dot{m}u_{out} = (\rho + d\rho)S(a - du)^2 \qquad (A1.8)$$

By inserting equations (A1.7) and (A1.8) in (A1.6), one obtains the relation (A1.9) when eliminating second order terms.

$$dP = 2\rho a du - a^2 d\rho \qquad (A1.9)$$

Using $d\rho$ from equation (A.1.4) and substituting in equation (A.1.9), one obtains (A1.10) which can be simplified and rewritten to express the change of velocity $du$ as per equation (A1.11)

$$dP = 2\rho a du - a^2\frac{\rho}{a}du \qquad (A1.10)$$

$$du = \frac{dP}{\rho a} \qquad (A1.11)$$

A1.11 is then integrated to obtain the velocity and combined to the equation of mass flow rate (equation (A1.0)) to obtain de final equation (A1.12):

$$\dot{m}(t) = \frac{S}{a}\int_0^t dP = \frac{S}{a}P(t) \qquad (A1.12)$$

## List of Acronyms, Abbreviations, and Symbols

| | |
|---|---|
| $a$ | Speed of sound in the fuel |
| A | Empirical constant in Equation 6 |
| $A_{nozzle}$ | Injector orifices, total area |
| B | Empirical constant in Equation 6 |
| BSFC | Brake Specific Fuel Consumption |
| C | Empirical constant in Equation 6 |
| $C_{D_{close}}$ | General equation for the closing phase of the instantaneous $C_d$ model |
| $C_{D, inj1, close}$ | Specific equation for the closing phase of injection 1 of the instantaneous $C_d$ model |
| $C_{D, inj2, close}$ | Specific equation for the closing phase of injection 2 of the instantaneous $C_d$ model |
| $C_{Dini, 2}$ | Discharge coefficient at beginning of second hydraulic injection |
| $C_{D_{lift}}$ | General equation for the opening phase of the instantaneous $C_d$ model |
| $C_{D, inj1, lift}$ | Specific equation for the opening phase of injection 1 of the instantaneous $C_d$ model |
| $C_{D, inj2, lift}$ | Specific equation for the opening phase of injection 2 of the instantaneous $C_d$ model |

| | | | |
|---|---|---|---|
| $C_{Dss}$ | Steady-state discharge coefficient | $t_{iod,fusion}$ | Modeled injector opening delay for single injection |
| CFD | Computational Fluid Dynamics | | |
| D | Empirical constant in Equation 6 | $t_{iodmax}$ | Maximum injector opening delay (obtained at 600 bar herein) |
| DT | Time interval between the beginning of each injection (second) | | |
| E | Empirical constant in Equation 4 | $t'$ | Time constant associated with moment when $C_d$ is equal to 0.1% of the closing delay |
| ECU | Engine Control Unit | | |
| ET | Injector energization time (second) | | |
| $ET1$ | Injector energization time – first injection (second) | $t^*$ | Adimensional injection time |
| | | $t_{11}$ | Start of hydraulic injection of first injection |
| $ET2$ | Injector energization time – second injection (second) | $t_{12}$ | Start of hydraulic injection of second injection |
| IOD | Experimental Injector Opening Delay | $t_{21}$ | Start of mass flow rate reduction phase of first injection |
| ICD | Experimental Injector Closing Delay | | |
| k | Empirical Constant in Equations 7 and 9 | $t_{22}$ | Start of mass flow rate reduction phase of second injection |
| $\dot{m}$ | mass flow rate | | |
| $m_f$ | Total injected mass | $t_{31}$ | Hydraulic end of first injection |
| $NO_x$ | Nitrous Oxides ($NO + NO_2$) | $t_{32}$ | Hydraulic end of second injection |
| $P_{back}$ | Backpressure | T | Peak flowrate continuity constant |
| $P_{inj}$ | Injection pressure | $\Delta P$ | Pressure difference between $P_{inj}$ and $P_{amb}$ |
| ROI | Rate of injection | $\rho_f$ | Fuel density |
| S | Inner tube surface area | $\tau$ | Combined time constant when both lift and close are approximated equal |
| $t_{icd}$ | Modeled injector closing delay for single injection | | |
| | | $\tau_{lift}$ | Time constant of injector to reach a steady-state mass flow rate |
| $t_{icd,fusion}$ | Modeled injector closing delay for single injection | | |
| | | $\tau_{close}$ | Characteristic needle closure time |
| $t_{iod}$ | Modeled injector opening delay for single injection | | |